

DSMS Telecommunications Link  
Design Handbook

---

202, Rev. A  
34-m and 70-m Doppler


December 15, 2002

---


Document Owner:

 12/17/02  
C. J. Ruggier Date  
Tracking System Engineer

Approved by:

 1/6/03  
J. B. Berner Date  
Telecommunication Service System  
Development Engineer

Author

 8/30/02  
P. W. Kinman Date

Released by:

[Signature on File]  
[at DSMS Library] 2/10/03  
DSMS Document Release Date

### ***Change Log***

<b>Rev</b>	<b>Issue Date</b>	<b>Affected Paragraphs</b>	<b>Change Summary</b>
Initial	11/30/2000	All	All
A	12/15/2002	Many	Added discussion of one-way Doppler error and X-Up/S-Down Solar Phase Scintillation errors. Renumbered all equations

### ***Note to Readers***

There are two sets of document histories in the 810-005 document that are reflected in the header at the top of the page. First, the overall document is periodically released as a revision when major changes affect a majority of the modules. For example, the original release of this document was part of Revision E. Second, the individual modules also change, starting as the initial issue that has no revision letter. When a module is changed, a change letter is appended to the module number on the second line of the header and a summary of the changes is entered in the module's change log.

## ***Contents***

<b><u>Paragraph</u></b>	<b><u>Page</u></b>
1. Introduction.....	4
1.1 Purpose.....	4
1.2 Scope.....	4
2. General Information .....	4
2.1 Doppler Measurement Error .....	7
2.1.1 Measurement Error for One-Way Doppler.....	9
2.1.2 Measurement Error for Two-Way and Three-Way Doppler .....	9
2.2 Carrier Tracking .....	10
2.2.1 Carrier Loop Bandwidth .....	10
2.2.2 Static Phase Error in the Carrier Loop.....	10
2.2.3 Carrier Phase Error Variance .....	11
2.2.4 Carrier Power Measurement .....	12
2.3 Doppler Measurement With Small Sun-Earth-Probe Angles .....	12
2.3.1 Doppler Measurement Error .....	13
2.3.2 Carrier Phase Error Variance .....	14
Appendix A References .....	20

## ***Illustrations***

<b><u>Figure</u></b>	<b><u>Page</u></b>
1. One-Way Doppler Measurement .....	6
2. Two/Three-Way Doppler Measurement.....	6
3. Doppler Measurement Error Due to Solar Phase Scintillation: S-Up/S-Down.....	15
4. Doppler Measurement Error Due to Solar Phase Scintillation: S-Up/X-Down .....	16
5. Doppler Measurement Error Due to Solar Phase Scintillation: X-Up/X-Down.....	17
6. Doppler Measurement Error Due to Solar Phase Scintillation: X-Up/S-Down .....	18
7. Doppler Measurement Error Due to Solar Phase Scintillation: X-Up/Ka-Down.....	19

## ***Table***

<b><u>Table</u></b>	<b><u>Page</u></b>
1. Static Phase Error.....	12

## **1.        *Introduction***

### **1.1        *Purpose***

This module provides sufficient information for the telecommunications engineer to understand the capabilities and limitations of the equipment used for Doppler measurement at the Deep Space Network (DSN) 34-m and 70-m stations.

### **1.2        *Scope***

The scope of this module is limited to those features of the Downlink Channel at the 34-m High-efficiency (34-m HEF), 34-m Beam Waveguide (34-m BWG), and 70-m stations that relate to the measurement of and reporting of the Doppler effect. This module does not discuss the capabilities of the equipment used for Doppler measurement at the DSN 34-m High-speed Beam Waveguide (HSB) station.

## **2.        *General Information***

The relative motion of a transmitter and receiver causes the received frequency to differ from that of the transmitter. This is the Doppler effect. In deep space communications it is usual to define Doppler as the transmitted frequency (the uplink) minus the received frequency (the downlink) divided by the ratio that was used onboard the spacecraft (the transponding ratio) to generate the downlink frequency. For the receding spacecraft that are typical of deep space exploration, the Doppler so defined is a positive quantity. Since the frequency of a carrier equals the rate-of-change of carrier phase, the Downlink Channel supports Doppler measurement by extracting the phase of the downlink carrier (Reference 1).

There are three types of Doppler measurement: one-way, two-way, and three-way. In all of these cases, the accumulating downlink carrier phase is measured and recorded. When the measurement is one-way, the frequency of the spacecraft transmitter must typically be inferred. A much more accurate Doppler measurement is possible when the spacecraft coherently transponds a carrier arriving on the uplink. In such a case, the downlink carrier frequency is related to the uplink carrier frequency by a multiplicative constant, the transponding ratio. Also, the downlink carrier phase equals the uplink carrier phase multiplied by this transponding ratio. Thus, when an uplink signal is transmitted by the DSN and the spacecraft coherently transponds this uplinked signal, a comparison of the uplink transmitter phase record with the downlink receiver phase record gives all the information necessary for an accurate computation of the combined Doppler on uplink and downlink. When one Deep Space Station (DSS) both provides the uplink and receives the downlink, so that there are two “nodes” (the DSS and the spacecraft) present, then it is a two-way measurement. When one DSS provides the uplink and another receives the downlink, so that there are three nodes present, then it is a three-way measurement.

Figure 1 illustrates one-way Doppler measurement. The measurement is referenced to the signal originating on the spacecraft. The frequency stability of the spacecraft

oscillator used to generate the downlink carrier will, in general, limit the performance of this Doppler measurement. Usually, only Ultra-Stable Oscillators (USOs) are used for one-way Doppler measurement.

Figure 2, Two/Three-Way Doppler Measurement, illustrates the more usual means of measuring Doppler. The measurement originates at a DSS. The uplink carrier frequency is synthesized within the exciter from a highly stable frequency reference provided by the Frequency and Timing Subsystem (FTS). Since this reference is much more stable than anything that a spacecraft-borne oscillator could provide, a two-way or three-way Doppler measurement is more accurate than a one-way measurement. The uplink carrier may be either constant or varied in accord with a tuning plan. In either case, the phase of the uplink carrier is recorded for use in the computation of a Doppler effect.

For all Doppler measurements (one-, two-, and three-way), the downlink signal is routed from the Antenna Feed/Low Noise Amplifier (LNA) to the Downlink Channel. This is reflected in Figures 1 and 2. Within the Radio-frequency to Intermediate-frequency Downconverter (RID), which is located at the antenna, a local oscillator is generated by frequency multiplication of a highly stable frequency reference from the FTS and the incoming downlink signal is heterodyned with this local oscillator. The Intermediate-Frequency (IF) signal that results is sent to the Signal Processing Center (SPC).

In the SPC, the IF to Digital Converter (IDC) alters the frequency of the IF signal by a combination of up-conversion and down-conversion to a final analog frequency of approximately 200 MHz and then performs analog-to-digital conversion. The final analog stage of down-conversion uses a local oscillator supplied by the Channel-Select Synthesizer (CSS), which is also part of the Downlink Channel. The CSS is adjusted before the beginning of a pass to a frequency appropriate for the anticipated frequency range of the incoming downlink signal. During the pass, the frequency of the CSS remains constant. The local oscillator frequencies of the CSS (and, indeed, of all local oscillators in the analog chain of down-conversion) are synthesized within the Downlink Channel from highly stable frequency references provided by the FTS. All analog stages of down-conversion are open-loop, and so the digital signal coming out of the IDC reflects the full Doppler effect on the downlink carrier.

The Receiver and Ranging Processor (RRP) accepts the signal from the IDC and extracts carrier phase with a digital phase-locked loop (Reference 2). The loop is configured to track the phase of a phase-shift keyed signal with residual carrier, a suppressed carrier, or a QPSK signal. Since every analog local oscillator is held at constant frequency during a pass, the downlink carrier phase at sky frequency (that is, the phase that arrives at the DSS antenna) is easily computed from the local oscillator frequencies and the time-varying phase extracted by the digital phase-locked loop.

Since Doppler is a difference of frequencies and a frequency is a derivative of phase, a record of phase transmitted on the uplink and of phase received on the downlink is sufficient to compute the combined uplink/downlink Doppler. It is important to note that these

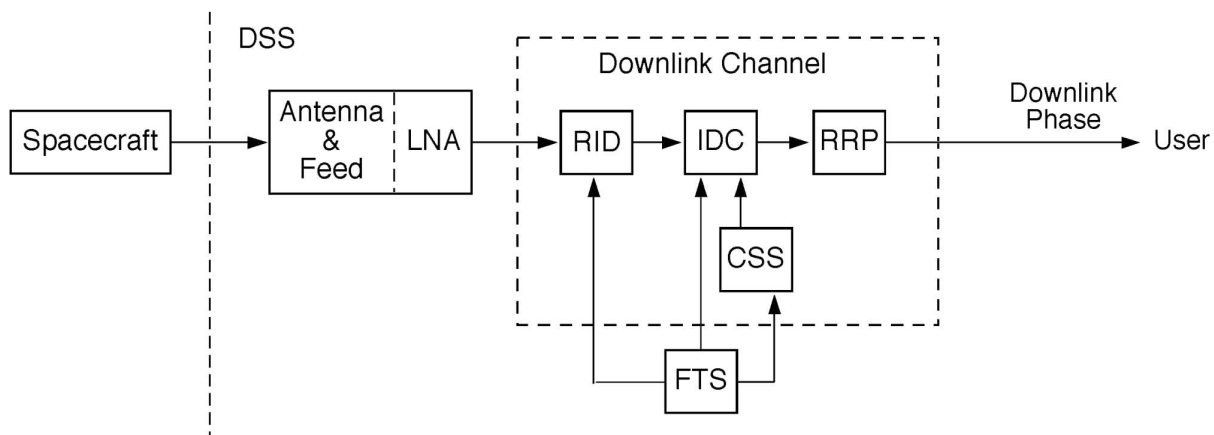


Figure 1. One-Way Doppler Measurement

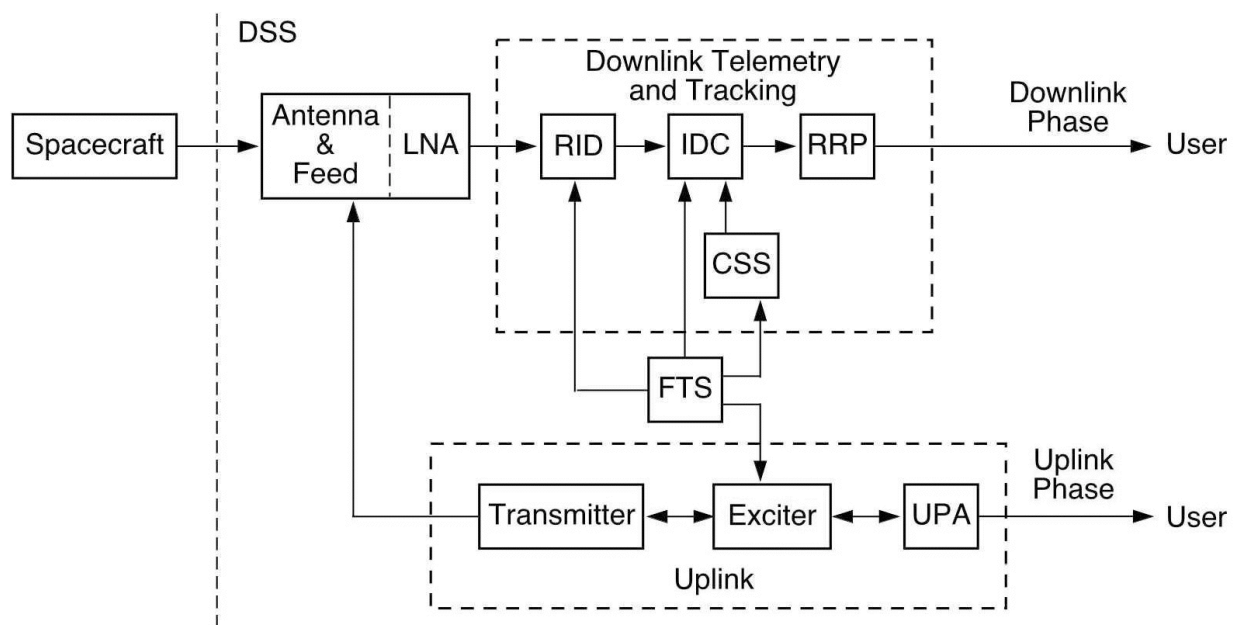


Figure 2. Two/Three-Way Doppler Measurement

phase records must account for integer as well as fractional cycles. (This is unlike many telecommunications applications where it is necessary to know the carrier phase only modulo one cycle.) The data are uplink and downlink phase counts at sky frequency (only downlink phase counts in the case of a one-way measurement). The downlink phase counts are available at 0.1-second intervals. The uplink phase counts are available from the Uplink Processor Assembly (UPA) at 1.0-second intervals.

## 2.1 *Doppler Measurement Error*

Only errors in measuring the rate-of-change of the distance between phase centers of the antennas are considered here. There are other errors that must be considered in any navigation solution, such as those introduced by propagation through the troposphere, the ionosphere, and the solar corona. Additional information on the effect of the solar corona on Doppler measurement is contained in paragraph 2.3.

Each error is characterized here as a standard deviation of range-rate  $\sigma_V$  and is in units of velocity. To translate any of these errors to a standard deviation of frequency  $\sigma_f$  the following equation can be used.

$$\sigma_f = \frac{2f_C}{c} \sigma_V \quad (1)$$

where

$$\begin{aligned} f_C &= \text{the downlink carrier frequency and} \\ c &= \text{the speed of light in vacuum.} \end{aligned}$$

Equation (1) is for two-way and three-way Doppler measurement. (The factor of 2 is absent for one-way Doppler measurement.)

When tracking a residual carrier, the carrier loop signal-to-noise ratio is

$$\rho_L = \left. \frac{P_C}{N_0} \right|_{D/L} \cdot \frac{1}{B_L} \quad (2)$$

where  $P_C/N_0|_{D/L}$  is the downlink carrier power to noise spectral density ratio, Hz.

There is an additional loss to the carrier loop signal-to-noise ratio when tracking a residual carrier with non-return-to-zero symbols in the absence of a subcarrier. This loss is due to the presence of data sidebands overlaying the residual carrier in the frequency domain and therefore increasing the effective noise level for carrier synchronization. In this case,  $\rho_L$  must be calculated as (Reference 3)

$$\rho_L = \left. \frac{P_C}{N_0} \right|_{D/L} \cdot \frac{1}{B_L} \cdot \frac{1}{1 + 2E_S/N_0} \quad (3)$$

where  $E_S/N_0$  is the energy per symbol to noise spectral density ratio.

When tracking a suppressed carrier, the carrier loop signal-to-noise ratio is

$$\rho_L = \left. \frac{P_T}{N_0} \right|_{D/L} \cdot \frac{S_L}{B_L} \quad (4)$$

where

$P_T/N_0|_{D/L}$  = downlink total signal power to noise spectral density ratio, Hz

$S_L$  = squaring loss of the Costas loop (Reference 4),

$$S_L = \frac{2 \frac{E_S}{N_0}}{1 + 2 \frac{E_S}{N_0}} \quad (5)$$

When tracking QPSK, the carrier loop signal-to-noise ratio is

$$\rho_L = \left. \frac{P_T}{N_0} \right|_{D/L} \cdot \frac{S_{LQ}}{B_L} \quad (6)$$

where  $S_{LQ}$  is the squaring loss of the QPSK Costas loop (Reference 5),

$$S_{LQ} = \frac{1}{1 + \frac{9}{2E_{SQ}/N_0} + \frac{6}{(E_{SQ}/N_0)^2} + \frac{3}{2(E_{SQ}/N_0)^3}}, \quad (7)$$

where  $E_{SQ}/N_0$  is the energy per quaternary channel symbol to noise spectral density ratio.

When telemetry data in a non-return to zero (NRZ) format directly modulate the carrier (that is, no subcarrier) and there is an imbalance in the data (that is, an unequal number of logical ones and zeros), a residual-carrier loop will experience an additional jitter. This jitter represents an additional error source for Doppler measurement. The size of this error contribution is strongly dependent on the statistics of the telemetry data.



### 2.1.1 *Measurement Error for One-Way Doppler*

Measurement error for one-way Doppler is normally dominated by the relative instability of the spacecraft oscillator and by the lack of knowledge of the exact frequency of this oscillator. Associated with one-way Doppler measurement is an unknown bias due to uncertainty in the transmitted frequency. In addition, there is a random error due to instability of the spacecraft oscillator. This latter error may be roughly modeled as

$$\sigma_V = \sqrt{2}c\sigma_y \quad (8)$$

where

- $\sigma_V$  = the standard deviation of range-rate in velocity units,
- $c$  = the speed of light in vacuum, and
- $\sigma_y$  = the Allan deviation of the spacecraft oscillator.

The Allan deviation is a function of integration time.

### 2.1.2 *Measurement Error for Two-Way and Three-Way Doppler*

Measurement errors for two-way coherent and three-way coherent Doppler must include the effect of jitter introduced by the spacecraft receiver. The two-way or three-way coherent Doppler measurement error due to thermal noise is approximated by

$$\sigma_V = \frac{c}{2\sqrt{2}\pi f_C T} \sqrt{\frac{1}{\rho_L} + \frac{G^2 B_L}{P_C/N_0|_{U/L}}} \quad (9)$$

where

- $T$  = measurement integration time, s
- $f_C$  = downlink carrier frequency, Hz
- $c$  = speed of light in vacuum, mm/s
- $G$  = transponding ratio
- $B_L$  = one-sided, noise-equivalent, loop bandwidth of downlink carrier loop, Hz
- $P_C/N_0|_{U/L}$  = uplink carrier power to noise spectral density ratio, Hz
- $\rho_L$  = downlink carrier loop signal-to-noise ratio.

Equation (9) assumes that the transponder (uplink) carrier loop bandwidth is large compared with the DSS (downlink) carrier loop bandwidth, which is typically the case.

## 2.2 *Carrier Tracking*

The Downlink Channel can be configured to track phase-shift keyed telemetry with residual carrier or a suppressed carrier or a QPSK signal. In order to achieve good Doppler measurement performance, it is important to characterize the phase error in the carrier loop.

### 2.2.1 *Carrier Loop Bandwidth*

The one-sided, noise-equivalent, carrier loop bandwidth is denoted  $B_L$ . The user may choose to change  $B_L$  during a tracking pass, and this can be implemented without losing phase-lock, assuming the change is not too large.

There are limits on the carrier loop bandwidth.  $B_L$  can be no larger than 200 Hz. The lower limit on  $B_L$  is determined by the phase noise on the downlink. In addition, when operating in the suppressed-carrier mode,  $B_L$  is subject to the following constraint.

$$B_L \leq \frac{R_{SYM}}{20}, \text{ suppressed carrier,} \quad (10)$$

where  $R_{SYM}$  is the telemetry symbol rate.

In general, the value selected for  $B_L$  should be small in order to maximize the carrier loop signal-to-noise ratio. On the other hand,  $B_L$  must be large enough that neither of the following variables becomes too large: the static phase error due to Doppler dynamics and the contribution to carrier loop phase error variance due to phase noise on the downlink. The best  $B_L$  to select will depend on circumstances. Often, it will be possible to select a  $B_L$  of less than 1 Hz. A larger value for  $B_L$  is necessary when there is significant uncertainty in the downlink Doppler dynamics, when the downlink is one-way (or two-way non-coherent) and originates with a less stable oscillator (such as an Auxiliary Oscillator), or when the Sun-Earth-probe angle is small (so that solar phase scintillations are present on the downlink).

When tracking a spinning spacecraft, it may be necessary to set the carrier loop bandwidth to a value that is somewhat larger than would otherwise be needed. The loop bandwidth must be large enough to track out the variation due to the spin. Also, the coherent AGC in the receiver must track out the amplitude variations.

The user may select either a type 2 or type 3 carrier loop. Both loop types are perfect, meaning that the loop filter implements a true accumulation.

### 2.2.2 *Static Phase Error in the Carrier Loop*

The carrier loop, with either a type 2 or type 3 loop, has a very large tracking range; even a Doppler offset of several megahertz can be tracked. With a finite Doppler rate, however, there will be a static phase error in a type 2 loop.

Table 1, Static Phase Error (rad), shows the static phase error in the carrier loop that results from various Doppler dynamics for several different loops. These equations are based on the work reported in Reference 6. The Doppler dynamics are here defined by the parameters  $\alpha$  and  $\beta$ .

$$\begin{aligned}\alpha &= \text{Doppler Rate (Hz/s)} \\ \beta &= \text{Doppler Acceleration (Hz/s}^2\text{)}\end{aligned}$$

In the presence of a persistent Doppler acceleration, a type 2 loop will periodically slip cycles.

The equations of Table 1 are valid when tracking phase-shift keyed telemetry with either residual or suppressed carrier or a QPSK signal. These equations are exactly the same as those appearing in Appendix C of module 207, 34-m and 70-m Telemetry.

### 2.2.3 *Carrier Phase Error Variance*

When the spacecraft is tracked one-way, the carrier phase error variance  $\sigma_\phi^2$  is given by

$$\sigma_\phi^2 = \frac{1}{\rho_L} + \sigma_S^2 \quad (11)$$

When the spacecraft is tracked in a two-way or three-way coherent mode, the carrier phase error variance  $\sigma_\phi^2$  is given by

$$\sigma_\phi^2 = \frac{1}{\rho_L} + \frac{G^2(B_{TR} - B_L)}{P_C/N_0|_{U/L}} + \sigma_S^2 \quad (12)$$

where

$$\begin{aligned}B_{TR} &= \text{one-sided, noise-equivalent, transponder carrier loop bandwidth, Hz} \\ \sigma_S^2 &= \text{contribution to carrier loop phase error variance due to solar phase} \\ &\quad \text{scintillations, rad}^2 \text{ (see paragraph 2.3.2)}\end{aligned}$$

and the other parameters are as defined in paragraph 2.1.2.

It is recommended that the following constraint on carrier phase error variance be observed.

$$\sigma_\phi^2 \leq \begin{cases} 0.10 \text{ rad}^2, & \text{residual carrier} \\ 0.02 \text{ rad}^2, & \text{suppressed carrier} \end{cases} \quad (13)$$

Table 1. Static Phase Error (rad)

<b>Loop</b>	<b>Constant Range-Rate</b>  $\left( \begin{array}{c} \text{Constant} \\ \text{Doppler Offset} \end{array} \right)$	<b>Constant Derivative of Range-Rate</b>  $\left( \begin{array}{c} \text{Constant} \\ \text{Doppler Rate} \end{array} \right)$	<b>Constant Second Derivative of Range-Rate</b>  $\left( \begin{array}{c} \text{Constant} \\ \text{Doppler Acceleration} \end{array} \right)$
type 2, standard underdamped	0	$\frac{9\pi}{16B_L^2} \cdot \alpha$	$\left( \frac{9\pi\beta}{16B_L^2} \right) t - \frac{27\pi\beta}{64B_L^3}$
type 2, supercritically damped	0	$\frac{25\pi}{32B_L^2} \cdot \alpha$	$\left( \frac{25\pi\beta}{32B_L^2} \right) t - \frac{125\pi\beta}{128B_L^3}$
type 3, standard underdamped	0	0	$\frac{12167\pi}{8000B_L^3} \cdot \beta$
type 3, supercritically damped	0	0	$\frac{35937\pi}{16384B_L^3} \cdot \beta$

#### 2.2.4 *Carrier Power Measurement*

When the downlink is residual-carrier, an estimate of the downlink carrier power  $P_C$  is available. When the downlink is suppressed-carrier, an estimate of the total downlink power  $P_T$  is available. This is done by first estimating  $P_C/N_0|_{D/L}$  (with a modified version of the algorithm described in Reference 7) or  $P_T/N_0|_{D/L}$  (with the split-symbol moments algorithm described in Reference 8). An estimate of the noise spectral density  $N_0$  comes from continual measurements made by a noise-adding radiometer. This information is used to compute absolute power  $P_C$  or  $P_T$ . The results are reported once per second.

#### 2.3 *Doppler Measurement With Small Sun-Earth-Probe Angles*

When the Sun-Earth-probe angle is small and the spacecraft is beyond the Sun, microwave carriers pick up phase scintillations in passing through the solar corona. There is a resulting contribution to Doppler measurement error and also an increase in the carrier loop phase error variance. The magnitudes of these effects are highly variable, depending on the activity of the Sun.

### 2.3.1 Doppler Measurement Error

Equations (14) and (15), below, based on the work reported in Reference 9, offer a coarse estimate of the average solar contribution to the standard deviation of Doppler measurement error. Equation (14) is valid when tracking phase-shift keyed telemetry with either residual or suppressed carrier or a QPSK signal, but only for Sun-Earth-Probe angles between 5° and 27°. In general, the standard deviation of Doppler measurement error will be the root-sum-square of the error standard deviation due to thermal noise, which is given in Equation (9), and the error standard deviation due to solar phase scintillations, which is given in Equation (14).

$$\sigma_V = \frac{0.73c\sqrt{C_{band}} \cdot [\sin(\theta_{SEP})]^{-1.225}}{f_C T^{0.175}} \quad (14)$$

where

- $T$  = the measurement integration time in seconds,
- $f_C$  = the downlink carrier frequency in hertz,
- $c$  = the speed of light in vacuum ( $\approx 3 \times 10^{11}$  mm/s), and
- $\theta_{SEP}$  = the Sun-Earth-probe angle.

The result,  $\sigma_V$ , will have the same units as  $c$ .

The constant  $C_{band}$  depends on the uplink/downlink bands; it is given by

$$C_{band} = \begin{cases} 6.1 \times 10^{-5}, & \text{S - up/S - down} \\ 4.8 \times 10^{-4}, & \text{S - up/X - down} \\ 2.6 \times 10^{-5}, & \text{X - up/S - down} \\ 5.5 \times 10^{-6}, & \text{X - up/X - down} \\ 5.2 \times 10^{-5}, & \text{X - up/K}_a \text{ - down} \\ 1.9 \times 10^{-6}, & \text{K}_a \text{ - up/X - down} \\ 2.3 \times 10^{-7}, & \text{K}_a \text{ - up/K}_a \text{ - down} \end{cases} \quad (15)$$

Figure 3 shows  $\sigma_V$  as a function of Sun-Earth-probe angle for two-way or three-way Doppler measurement with an S-band uplink and an S-band downlink. The vertical axis is in units of mm/s. The three curves in that figure correspond to measurement integration times of 5, 60, and 1000 seconds. Figure 4 shows  $\sigma_V$  for an S-band uplink and an X-band downlink. Figure 5 shows  $\sigma_V$  for an X-band uplink and an X-band downlink. Figure 6 shows  $\sigma_V$  for an X-band uplink and an S-band downlink. Figure 7 shows  $\sigma_V$  for an X-band uplink and a K<sub>a</sub>-band downlink.

### 2.3.2 Carrier Phase Error Variance

Equation (16), below, based on the work reported in Reference 9, offers a coarse estimate of the average solar contribution, in units of  $\text{rad}^2$ , to carrier loop phase error variance. Equation (16) is valid when tracking phase-shift keyed telemetry with either residual or suppressed carrier or a QPSK signal, but only for Sun-Earth-Probe angles between  $5^\circ$  and  $27^\circ$ .

$$\sigma_S^2 = \frac{C_{band} \cdot C_{loop}}{(\sin \theta_{SEP})^{2.45} \cdot B_L^{1.65}}, \quad 5^\circ \leq \theta_{SEP} \leq 27^\circ \quad (16)$$

In Equation (16),  $\theta_{SEP}$  is the Sun-Earth-probe angle and  $B_L$  is the carrier loop bandwidth.  $C_{band}$  is given by Equation (15) for two-way and three-way coherent operation and by

$$C_{band} = \begin{cases} 2.6 \times 10^{-5}, & \text{S - down} \\ 1.9 \times 10^{-6}, & \text{X - down} \\ 1.3 \times 10^{-7}, & \text{K}_a \text{ - down} \end{cases} \quad (17)$$

for non-coherent operation.

$C_{loop}$  is a constant depending on the type of carrier loop selected.

$$C_{loop} = \begin{cases} 5.9, & \text{standard underdamped type 2 loop} \\ 5.0, & \text{supercritically damped type 2 loop} \\ 8.2, & \text{standard underdamped type 3 loop} \\ 6.7, & \text{supercritically damped type 3 loop} \end{cases} \quad (18)$$

Equation (16) together with Equations (15), (17), and (18) give the contribution of solar coronal phase scintillation to carrier loop phase error variance. It is used in Equation (12) to compute the total carrier loop phase error variance.

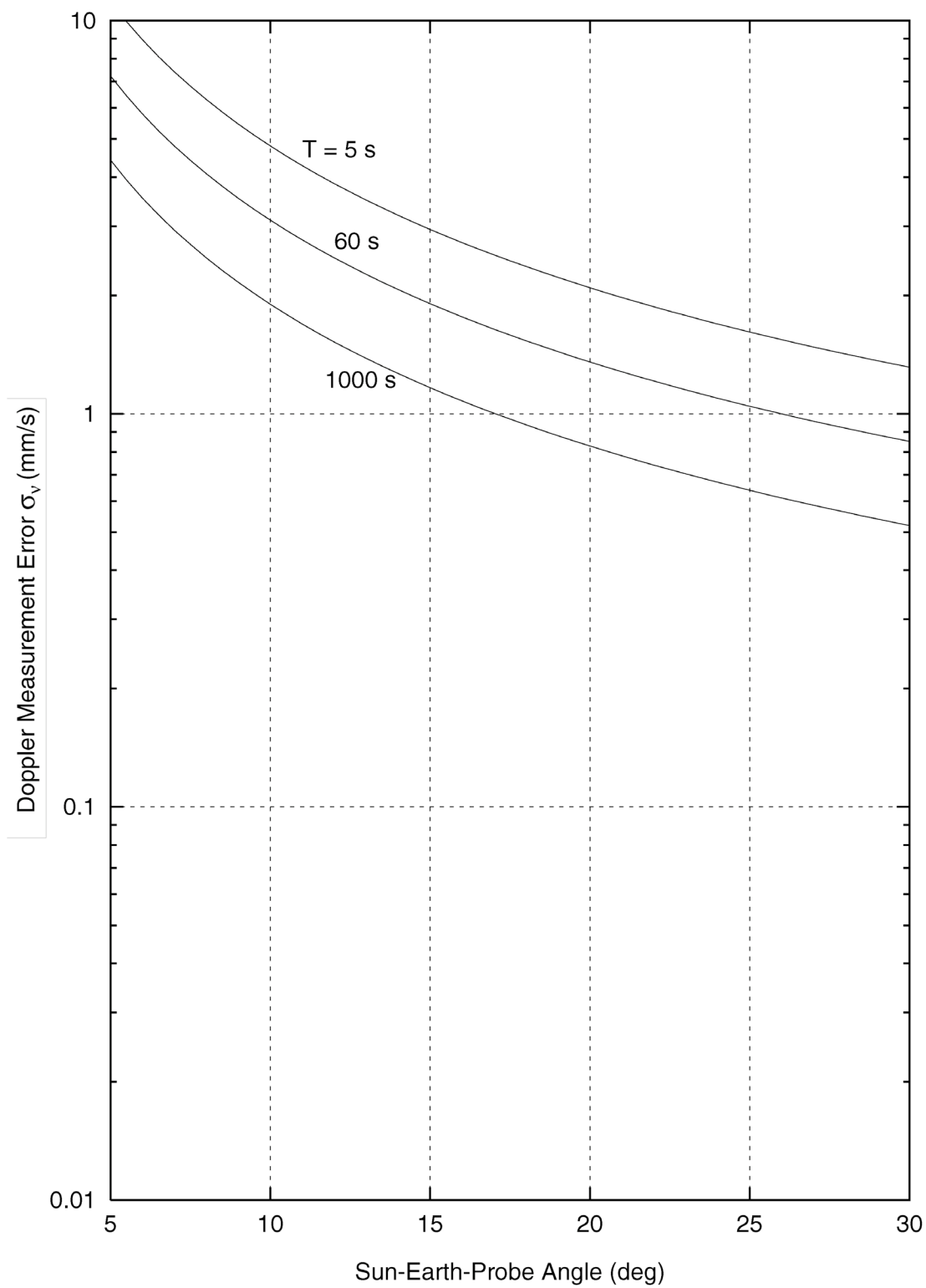


Figure 3. Doppler Measurement Error Due to Solar Phase Scintillation: S-Up/S-Down

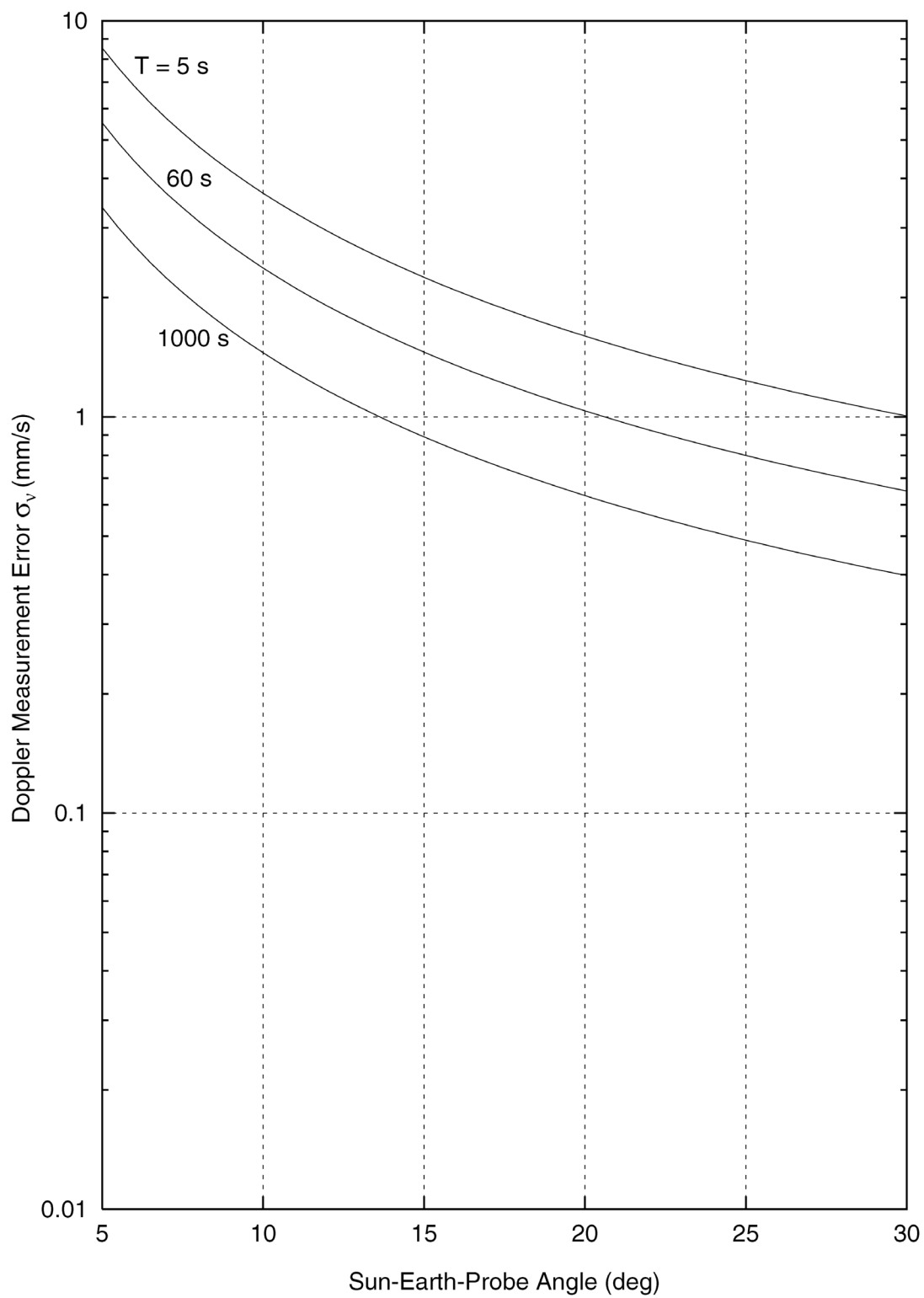


Figure 4. Doppler Measurement Error Due to Solar Phase Scintillation: S-Up/X-Down



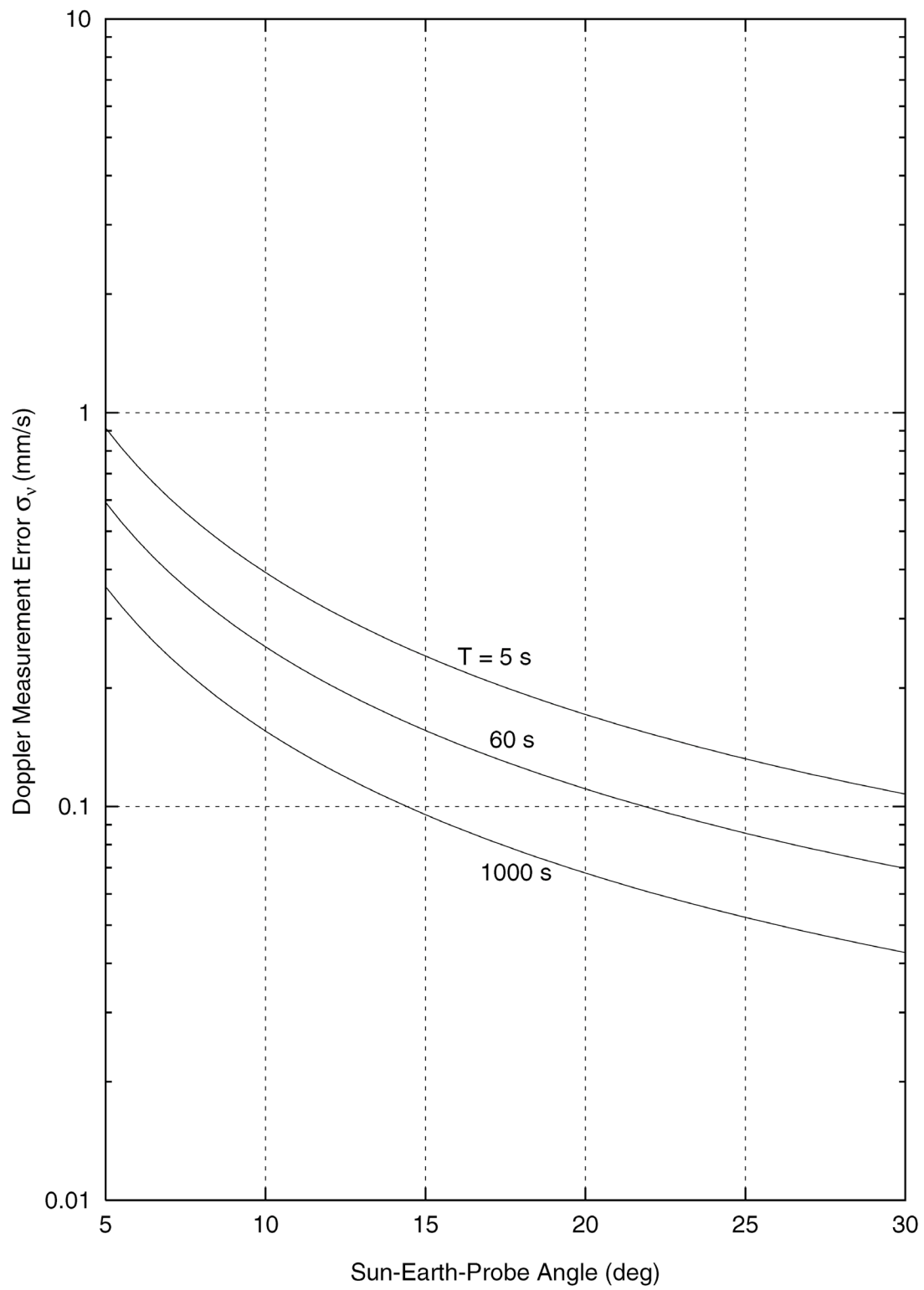


Figure 5. Doppler Measurement Error Due to Solar Phase Scintillation: X-Up/X-Down

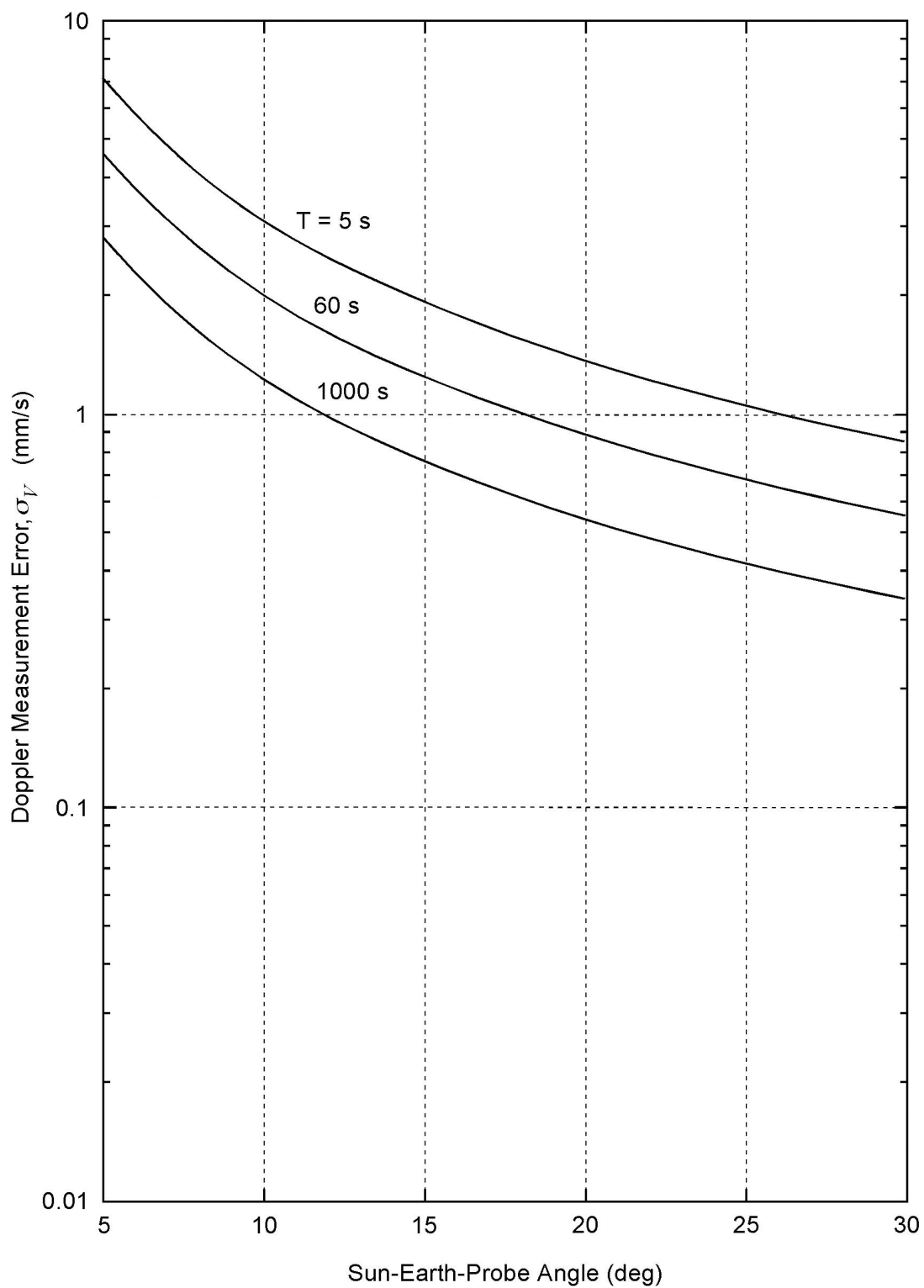


Figure 6. Doppler Measurement Error Due to Solar Phase Scintillation: X-Up/S-Down

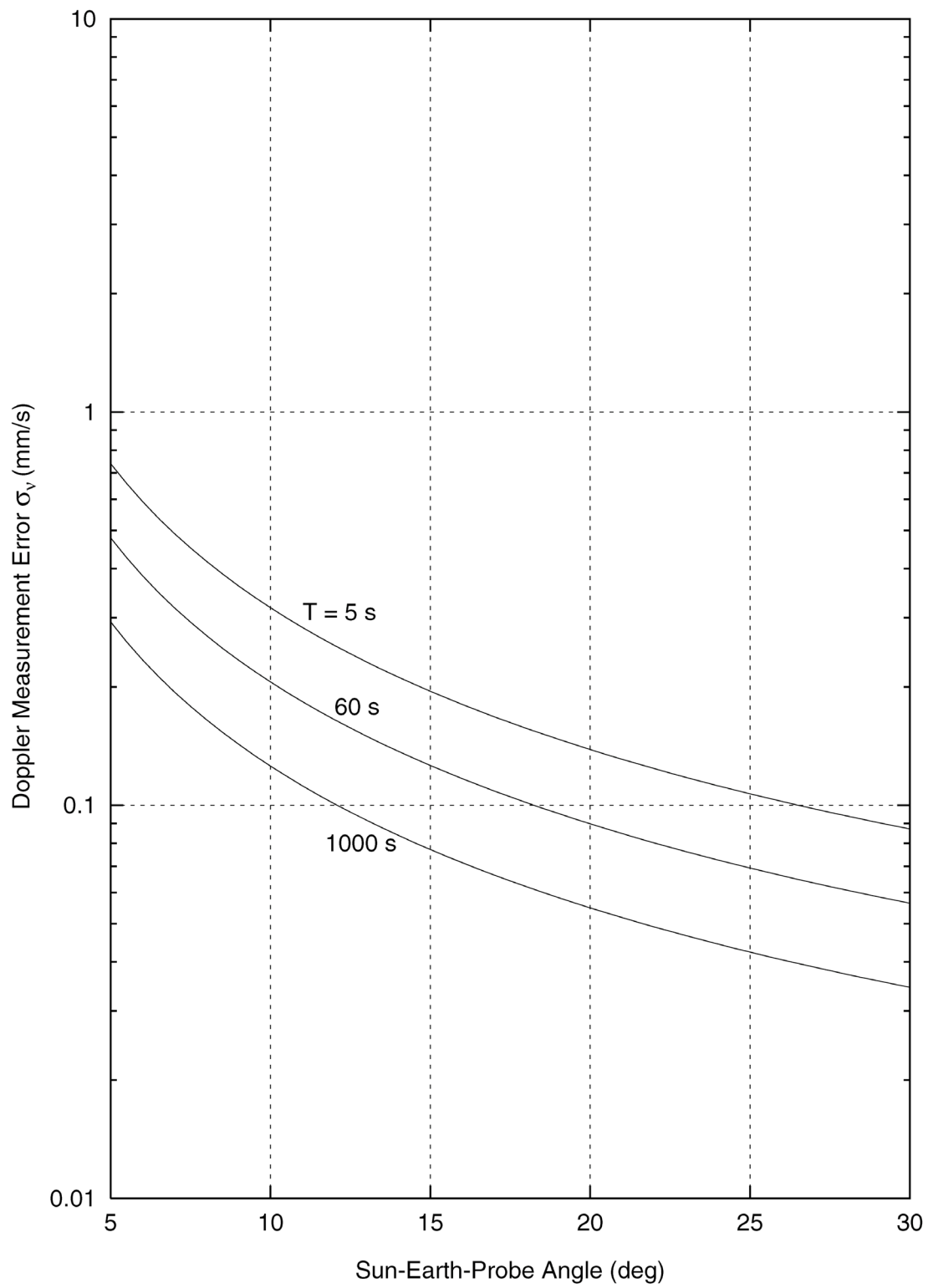


Figure 7. Doppler Measurement Error Due to Solar Phase Scintillation: X-Up/Ka-Down

## ***Appendix A***

### ***References***

1. P. W. Kinman, "Doppler Tracking of Planetary Spacecraft," *IEEE Transactions on Microwave Theory and Techniques*, Vol. 40, No. 6, pp. 1199-1204, June 1992.
2. J. B. Berner and K. M. Ware, "An Extremely Sensitive Digital Receiver for Deep Space Satellite Communications," *Eleventh Annual International Phoenix Conference on Computers and Communications*, pp. 577-584, Scottsdale, Arizona, April 1-3, 1992.
3. J. Lesh, "Tracking Loop and Modulation Format Considerations for High Rate Telemetry," *DSN Progress Report 42-44*, Jet Propulsion Laboratory, Pasadena, CA, pp. 117-124, April 15, 1978.
4. M. K. Simon and W. C. Lindsey, "Optimum Performance of Suppressed Carrier Receivers with Costas Loop Tracking," *IEEE Transactions on Communications*, Vol. COM-25, No. 2, pp. 215-227, February 1977.
5. J. H. Yuen, editor, *Deep Space Telecommunications Systems Engineering*, Plenum Press, New York, pp. 94-97, 1983.
6. S. A. Stephens and J. B. Thomas, "Controlled-Root Formulation for Digital Phase-Locked Loops," *IEEE Transactions on Aerospace and Electronic Systems*, Vol. 31, No. 1, pp. 78-95, January 1995.
7. A. Monk, "Carrier-to-Noise Power Estimation for the Block-V Receiver," *TDA Progress Report 42-106*, Jet Propulsion Laboratory, Pasadena, CA, pp. 353-363, August 15, 1991.
8. S. Dolinar, "Exact Closed-Form Expressions for the Performance of the Split-Symbol Moments Estimator of Signal-to-Noise Ratio," *TDA Progress Report 42-100*, pp. 174-179, Jet Propulsion Laboratory, Pasadena, CA, February 15, 1990.
9. R. Woo and J. W. Armstrong, "Spacecraft Radio Scattering Observations of the Power Spectrum of Electron Density Fluctuations in the Solar Wind," *Journal of Geophysical Research*, Vol. 84, No. A12, pp. 7288-7296, December 1, 1979.